The role of radial particle pinches in ELM suppression by resonant magnetic perturbations

The role of radial particle pinches in ELM suppression by resonant magnetic perturbations

W.M. Stacey[1] **and T.E. Evans**[2]

[1] Georgia Institute of Technology, Atlanta, GA 30332, USA
[2] General Atomics, San Diego, CA 92186, USA

Abstract

The force balance in the plasma edge in a matched pair of DIII-D (Luxon 2002 *Nucl. Fusion* **42** 6149) tokamak discharges with and without resonant magnetic perturbations (RMPs) is evaluated in order to investigate the effects on particle transport of RMP applied for the purpose of suppressing edge-localized modes (ELMs). Experimental data are used to evaluate the radial and toroidal force balances, which may be written as a pinch–diffusion relation for the radial ion flux to facilitate investigation of transport effects. The radial electric field in the H-mode plasma had a sharp negative dip in the steep gradient region of the edge pedestal, associated with which was a large inward pinch velocity. The main effect of RMP was to make the edge electric field less negative or more positive, reducing this strong negative dip in the radial electric field (even reversing it from negative to positive over some regions), thereby reducing the strong inward particle pinch in the edge of an H-mode discharge, thus causing a reduction in edge density below the ELM threshold.

(Some figures in this article are in colour only in the electronic version)

1. Introduction

Type-I edge-localized modes [1] (ELMs) pose a significant concern in magnetically confined toroidal fusion plasmas because they can rapidly erode plasma facing surfaces, reduce the coupling efficiency of radiofrequency antennas and cause noise in feedback circuits used to control magnetohydrodynamic (MHD) modes. ELMs are completely suppressed in the DIII-D tokamak [2] over a wide range of pedestal collisionalities [3] ($\nu_e^* = q_{95} R \varepsilon^{-3/2} (\upsilon_{Te} \tau_e)^{-1}$) and mitigated in the JET Tokamak [4] using resonant magnetic perturbation (RMP) fields [5–9] produced by non-symmetric coils located outside the vacuum vessel behind the plasma facing graphite tiles used to protect the vacuum vessel walls. Here R is the major radius, a is the minor radius, $\varepsilon \equiv a/R$ is the inverse aspect ratio, υ_{Te} is the electron thermal velocity, τ_e is the electron collision time and q_{95} is the safety factor at the 95% flux surface.

In high average triangularity $\delta = (\delta_{up} + \delta_{low})/2 \approx 0.53$ plasmas with moderately high collisionality ($\nu_e^* \approx 1$) and properly configured RMP fields, Type-I ELMs are replaced by small intermittent events with a coherent amplitude of modulation of $\approx$130 Hz, [5, 6]. In these discharges, an RMP field with a toroidal mode number $n = 3$ and a peak vacuum field amplitude approximately equal to that of the DIII-D field

errors in the edge plasma creates a dense set of vacuum field magnetic islands across the pedestal region. These islands are produced by the flux surface normal components of the RMP field from the DIII-D I-coil [10] with poloidal mode numbers ranging from $m = 9$ to $m = 14$ across the pedestal when the safety factor of the 95% normalized flux surface, q_{95}, is between 3.5 and 3.9 [6]. When this q_{95} resonant condition is satisfied, ELMs are suppressed by the applied RMP without any appreciable change in the pedestal pressure profile [5], suggesting that the RMP may couple directly to the eigenmode structure of the ELMs, which then changes the stability of the modes. Naturally occurring small (type-V) ELMs seen on NSTX [11] appear to share similar properties with the 130 Hz oscillations seen during moderate collisionality ELM suppression experiments in DIII-D.

During ELM suppression in moderate to high collision-ality DIII-D plasmas ($\nu^* > 1$) with $q_{95} \sim 3.7$, the I-coil currents are configured such that the upper and lower coils at the same toroidal angle have opposite polarities (referred to as up–down asymmetirc or odd parity), which produces resonant components that are approximately eight times smaller than the up-down symmetric (even parity) I-coil configuration. The odd parity configuration tends to produce larger non-resonant components as well. In these high collisionality cases, ELM suppression is in a q_{95} resonant window between

3.6 and 3.9. Outside this resonant window the $n = 3$ I-coil per-turbation field has little or no effect on the ELM frequency or amplitude. This behaviour is different from that seen in low-collisionality plasmas ($\nu^* < 0.3$) where even parity $n = 3$ pertrubation fields suppress ELM inside the resonant q_{95} win-dow (3.55–3.85) and mitigate ELMs (increase their frequency and reduce their amplitude) outside the q_{95} resonant window.

In low-collisionality plasmas with $\nu_e^* \leqslant 0.2$ and $\delta = 0.26$, ELMs are completely eliminated over a q_{95} resonant window ranging from 3.55 to 3.85 [7, 8, 12]. The minimum $m, n = 11, 3$ vacuum RMP field required for ELM suppression under these conditions lies between $\delta b_r^{(11,3)}/B_T = 1.7 \times 10^{-4}$ and $\delta b_r^{(11,3)}/B_T = 2.6 \times 10^{-4}$ for I-coil currents of 2 kA and 3 kA, respectively [7, 12]. Here B_T is the toroidal magnetic field on axis. This vacuum RMP field amplitude is approximately nine times larger than that required for the $\delta = 0.56$ with $\nu_e^* \approx 1$ case. In these low collisionality plasmas, ELMs are suppressed during a reduction in the pedestal pressure profile. The pedestal pressure is reduced due to a reduction in the density without appreciably affecting the electron thermal transport. The density reduction is controlled by the amplitude of the I-coil current along with other plasma parameters such as plasma shape, neutral beam heating power, collisionality, wall conditions and normalized plasma pressure (β_N) [8, 13]. This change in the pressure profile moves the edge pedestal into a stable peeling–ballooning mode operating region [14, 15].

We have previously investigated the differences in transport produced by the RMP by inferring [16] the edge plasma thermal diffusivities in an ELMing H-mode discharge and in an otherwise identical discharge with RMP fields. We found substantial reduction in ion thermal diffusivity with RMP fields but no significant difference in electron thermal diffusivity. This led us to conclude that the main effect of RMP was to reduce the average pedestal density relative to an H-mode discharge and thus to reduce the edge pressure below the ELM onset threshold.

Our purpose in this paper is now to investigate the mechanisms by means of which RMP fields affect this density reduction. To this end, we examine ion particle transport in the plasma edge of the same pair of discharges for which the investigation of thermal diffusivity differences was carried out. We use experimental data to evaluate the differences in force balance in the plasma edge for the two discharges, which differ in machine and plasma parameters only by the presence or absence of the RMP. The force balance can be formulated [17] as a pinch–diffusion relation for the radial particle flux of ions, which lends itself to an interpretation of differences in particle transport due to differences in the particle diffusion coefficient and the particle pinch velocity, both of which can be evaluated from experimental data (for the most part).

2. Matching ELM-suppressed RMP and ELMING H-mode discharges

A matched pair of low colllisionality, lower single null divertor discharges with plasma currents of 1.5 MA and toroidal field 2.0 T were configured for strong pumping in the lower divertor. In the H-mode discharge (without RMP), the data were averaged over the last 20% of successive inter-ELM intervals
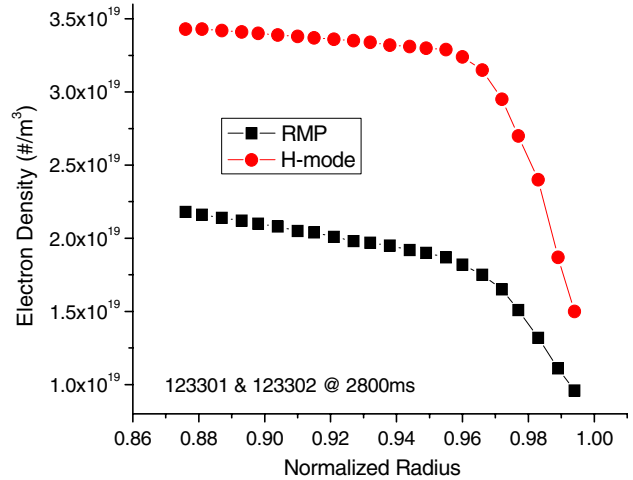

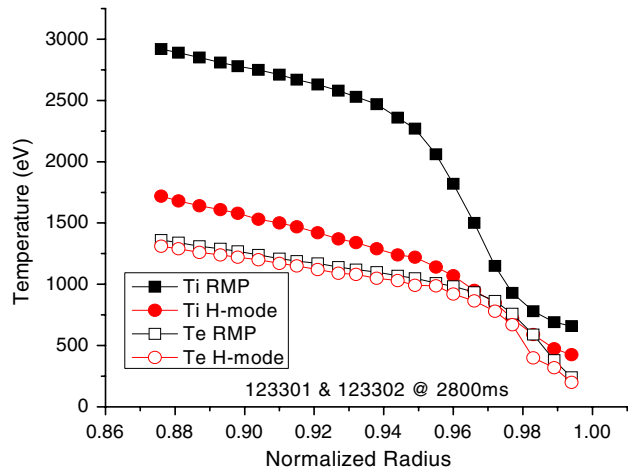**Figure 1.** Measured electron density (Thomson) profiles.

Figure 2. Measured electron (Thomson) and ion (CER) temperature profiles.

(to minimize the effect of the ELMs and random errors) at about 2800 ms into the discharge. The electron densities, the ion and electron temperatures, the radial electric field constructed from carbon pressure and rotation measurements and the carbon rotation measurements are shown for the edge plasma in figures 1–4. The density decrease, ion temperature and toroidal rotation velocity increase and the reduction in the negative radial electric field for the RMP discharge relative to the H-mode discharge are notable.

3. Experimentally inferred thermal diffusivities

For the sake of completeness, the inference of thermal dif-fusivities from experimental measurements of the temperature distribution has been repeated (incorporating some refinements in the methodology since [16]), and the results are plotted in figure 5. The RMP coil does not affect the electron thermal dif-fusivity, but reduces the ion thermal diffusivity substantially, with the result that the electron temperatures are similar in the H-mode and RMP shots but the ion temperature is substantially larger in the RMP shot (see figure 2).
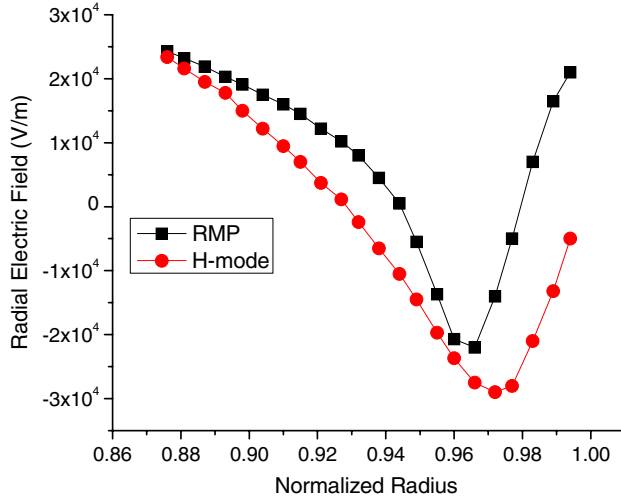
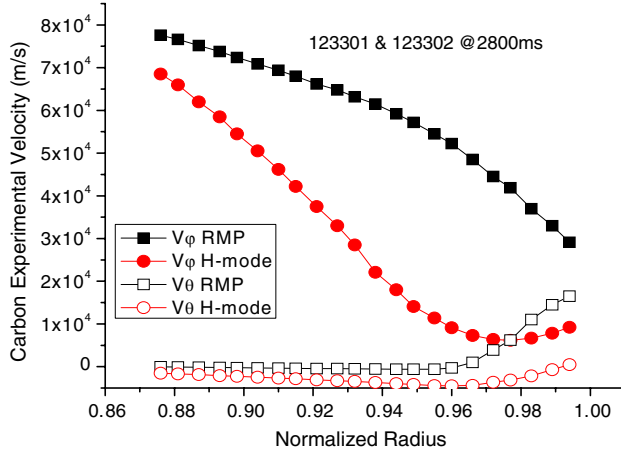**Figure 3.** Experimental radial electric field (constructed from carbon pressure and rotation measurements).
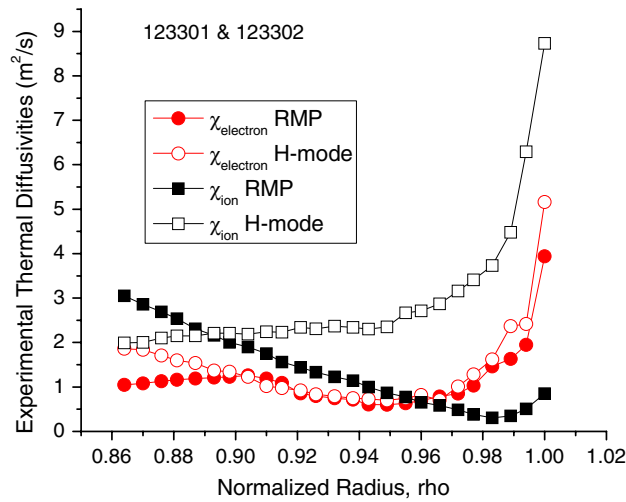

Figure 4. Measured carbon rotation velocities (CER).

Figure 5. Inferred experimental ion and electron thermal diffusivities.

4. Force balance and particle transport

The toroidal and radial momentum balance equations may be written as

$$n_j m_j [(\nu_{jk} + \nu_{dj}) V_{\phi j} - \nu_{jk} V_{\phi k}] = n_j e_j E_\phi^A + n_j e_j B_\theta V_{rj} + M_{\phi j} \tag{1}$$

and

$$V_{\phi j} = \frac{1}{B_\theta} \left[E_r + V_{\theta j} B_\phi - \frac{1}{n_j e_j} \frac{\partial p_j}{\partial r} \right], \tag{2}$$

where 'j' refers to the main deuterium ions and 'k' refers to the carbon impurity species, the superscript 'A' indicates this is the electromagnetic component of the electric field, and the quantity ν_{dj} is a toroidal angular momentum transfer frequency which represents the combined effect of viscosity, inertia, atomic physics and other 'anomalous' processes. The atomic physics terms are of this form and justification for representing the perpendicular- and gyro-viscous and the inertial toroidal momentum transfer processes in this form is discussed in [18]. $M_{\phi j}$ is the toroidal momentum input, and the other symbols have their usual meaning.

Equations (1) and (2) may be rearranged to obtain [17, 19] a pinch–diffusion relation for the main ion radial particle flux that provides insight as to the physical effect of the various forces on ion particle transport

$$\Gamma_j \equiv n_j V_{rj} = -\frac{n_j \widehat{D}_j}{p_j} \frac{\partial p_j}{\partial r} + n_j V_{rj}^{pinch}$$

$$= -\widehat{D}_j \left(\frac{\partial n_j}{\partial r} + \frac{n_j}{T_j} \frac{\partial T_j}{\partial r} \right) + n_j V_{rj}^{pinch}, \tag{3}$$

where the diffusion coefficient that follows from force balance is

$$\widehat{D}_j \equiv \frac{m_j T_j \nu_{jk}}{(e_j B_\theta)^2} \left(1 + \frac{\nu_{dj}}{\nu_{jk}} - \frac{e_j}{e_k} \right) \tag{4}$$

and

$$V_{rj}^{pinch} \equiv [-M_{\phi j} - n_j e_j E_\phi^A + n_j m_j (\nu_{jk} + \nu_{dj})$$
$$\times (f_p^{-1} V_{\theta j} + E_r / B_\theta) - n_j m_j \nu_{jk} V_{\theta k}][n_j e_j B_\theta]^{-1} \tag{5}$$

is identified as a 'velocity pinch' that is required by force balance. The external momentum input, which is a small term in equation (5) in the edge, can be calculated from the known beam geometry and power input. The induced toroidal electric field, which is also a small term, can be determined from the measured loop voltage. The density, temperature, radial electric field and carbon (k) toroidal rotation velocity are measured, and ν_{jk} can be calculated using the measured density and temperature. The radial momentum transfer frequency ν_{dj} can be inferred from experiment, as discussed in the following section, leaving the deuterium poloidal velocity as the only quantity which cannot be experimentally determined. We will use the measured carbon poloidal velocity as a surrogate for the deuterium poloidal rotation velocity in order to obtain a conservative lower bound on the pinch velocity evaluated from equation (5), as discussed in the appendix.
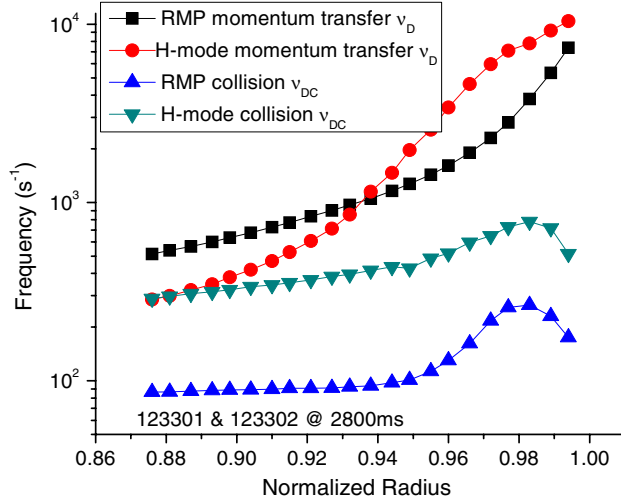
Figure 6. Inferred momentum transfer frequency and collision frequencies evaluated with measured temperatures and densities.

Figure 7. Deuterium particle diffusion coefficient inferred using measured data.

5. Inference of the momentum transfer frequency from experiment

Since the deuterium rotation velocities are not measured, we make use of a perturbation analysis [17, 19] in which $(V_{\phi j} - V_{\phi k})$ is taken as a small parameter to derive expressions which may be used to evaluate the experimental deuterium (j) and carbon (k) toroidal angular momentum transfer frequencies

$$\nu_{dj} = \tag{6}$$
$$\frac{(n_j e_j E_\phi^A + e_j B_\theta \Gamma_j + M_{\phi j}) + (n_k e_k E_\phi^A + e_k B_\theta \Gamma_k + M_{\phi k})}{(n_j m_j + n_k m_k) V_{\phi k}^{\exp}}$$

for the main deuterium ions and

$$\nu_{dk} = \frac{(n_k e_k E_\phi^A + e_k B_\theta \Gamma_k + M_{\phi k}) + n_j m_j \nu_{jk}(V_{\phi j} - V_{\phi k})_0}{n_k m_k V_{\phi k}^{\exp}} \tag{7}$$

for the carbon impurity ions, where

$$(V_{\phi j} - V_{\phi k})_0 = \frac{(n_j e_j E_\phi^A + e_j B_\theta \Gamma_j + M_{\phi j}) - n_j m_j \nu_{dj} V_{\phi k}^{\exp}}{n_j m_j (\nu_{jk} + \nu_{dj})} \tag{8}$$

is the first-order perturbation estimate of the difference in deuterium and carbon toroidal rotation velocities. Evaluation of equation (8) using the data for the RMP shot 123301 reveals that this velocity difference is in fact small compared with the measured carbon rotation [7], confirming the validity of the perturbation analysis. We also find that the perturbation approximation is valid for the H-mode shot 123302 during the time interval considered for this paper. The values of the radial particle fluxes needed to evaluate equations (6) and (7) were obtained by solving the continuity equation, using the measured densities and temperatures and calculated neutral beam and recycling neutral sources. The inferred angular momentum transfer frequencies are plotted in figure 6. The similar values of the inferred cross-field toroidal momentum transfer frequencies ν_{dj} for the two shots are consistent with the experimental observation that both the H-mode and RMP shots have the same neutral beam torque input and the H-mode
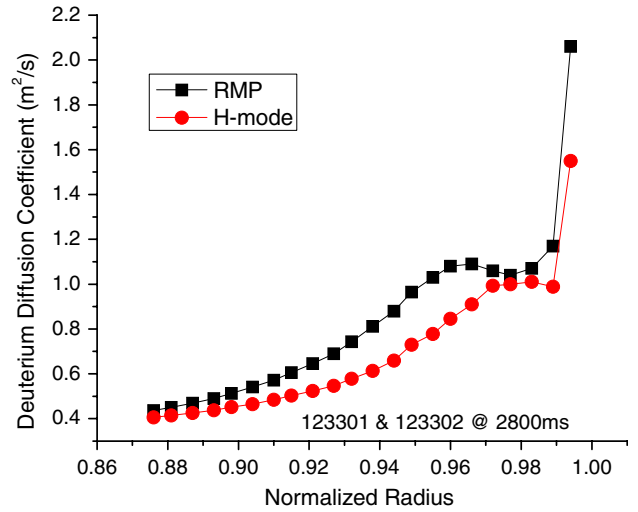
shot has about twice the density and somewhat less than half the toroidal rotation velocity of the RMP shot.

The collision frequencies for both shots are also plotted in figure 6.

6. Diffusion coefficients, pinch velocities and particle transport

The diffusion coefficient obtained by using the momentum transfer and collision frequencies shown in figure 6 and the ion temperature profiles shown in figure 2 are plotted in figure 7. The larger ion temperature for the RMP discharge is the main reason for the larger diffusion coefficient of that discharge. This larger diffusion coefficient would lead to a larger outward diffusive particle flux in the RMP discharge, but this effect is mitigated by the fact that the pressure gradient is also reduced in the RMP discharge relative to the H-mode discharge. The net radial particle fluxes calculated were outward in both cases but larger for the RMP discharge than for the H-mode discharge.

The data shown in figures 1–4 and the inferred momentum transfer frequency shown in figure 6 were used to evaluate the forces entering the pinch velocity expression given by equation (5). The contributions of the various forces and the resultant net pinch velocity is shown in figure 8 for the H-mode discharge and in figure 9 for the RMP discharge. In both these discharges, the force associated with the radial electric field was a major factor in determining the pinch velocity, although the $V_\theta \times B_\phi$ force was somewhat larger and of the opposite sign to the E_r force just inside the separatrix in the RMP discharge. The contributions of the $V_\phi \times B_\theta$, E_ϕ^A and M_ϕ forces were small. The net result in the H-mode discharge was a large inward pinch velocity almost entirely due to the radial electric field. The main effects of RMP were to make the edge electric field less negative or more positive, reducing the strong negative dip in the radial electric field (even reversing it from negative to positive over some regions), and to strengthen and reverse the poloidal rotation, with the net result of significantly reducing the strong inward pinch in the RMP relative to the H-mode discharge, as summarized in figure 10.
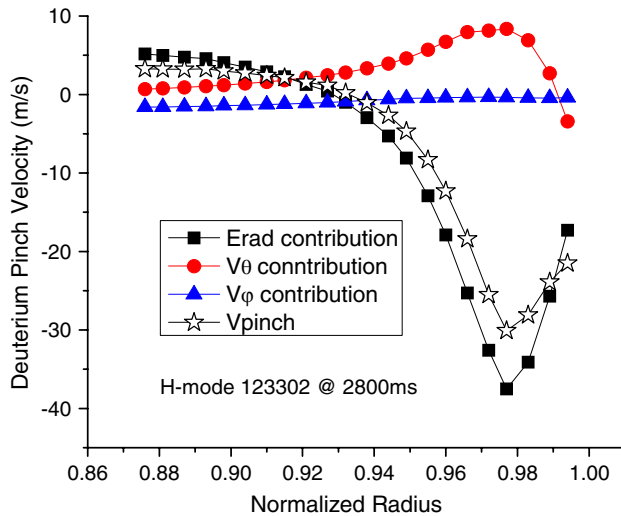
Figure 8. Deuterium radial pinch velocity inferred using measured data for H-mode discharge.
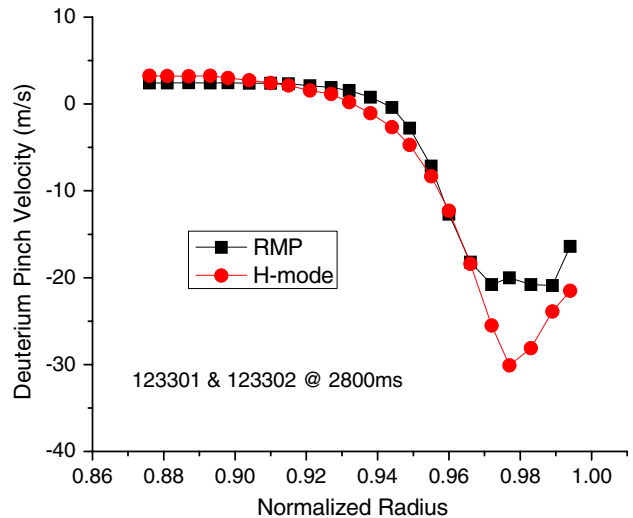

Figure 10. Comparison of inward deuterium radial pinch in H-mode and RMP.

reduction in inward pinch was due primarily to the change in direction of the electric field over a significant part of the edge pedestal, but changes in poloidal rotation due to the RMP were also important.

It appears that the radial electric field and the poloidal velocity are knobs for density control. Further investigations are obviously in order to understand how the RMP affects the radial electric field and poloidal rotation. An even more intriguing area for future exploration is the search for other possible means to control the radial electric field and the poloidal rotation in the plasma edge, thereby to achieve density control and ELM suppression by reducing the large inward velocity pinch in the edge of an H-mode plasma.
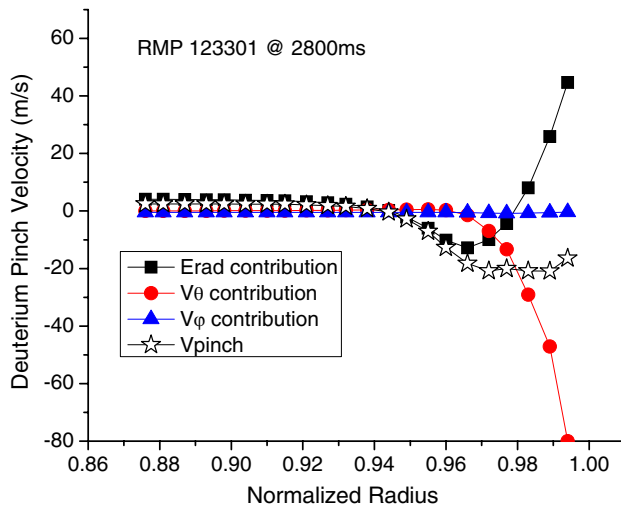
Figure 9. Deuterium radial pinch velocity inferred using measured data for RMP discharge.

We note that previous studies in limiter plasmas with applied static RMP fields have shown an increase in the poloidal and toroidal rotation that are consistent with a torque produced by a radial ion current driven by a change in E_r [20] and related changes in the particle confinement time [21]. We also note previous theoretical modelling work [22, 23] that emphasizes the role of E_r and V_θ in determining the particle transport due to RMPs. Another interesting result is the experimental identification [24, 25] and theoretical discussion [26] of the effects of diamagnetic drifts on the penetration physics of RMPs in TEXTOR.

7. Discussion

The major effect of the RMP in this study is to reduce the density below the ELM threshold by reducing the stronger inward particle pinch that would otherwise be present in an H-mode discharge, and by increasing the particle diffusion coefficient in the RMP discharge. In this RMP discharge, the

Appendix. Evaluation of deuterium poloidal rotation velocity

In order to evaluate the collection of forces constituting the pinch velocity, it is necessary to evaluate the deuterium poloidal rotation velocity, which is not measured. We have set the deuterium poloidal velocity equal to the measured carbon poloidal velocity for this purpose in order to obtain a conservative lower bound on the magnitude of the pinch velocity (as explained in the following), even though there is theoretical and experimental evidence that the two velocities may be of different signs and magnitudes under certain conditions.

There are a number of multi-fluid models for the poloidal rotation velocity (many of them summarized in [27]), all based on the poloidal momentum balance, but with different assumptions of which terms must be retained and with different constitutive relations for friction and parallel viscosity coefficients evaluated from kinetic theory. The lead author and his colleagues have made numerous calculations of carbon and deuterium poloidal velocities over the years for models of DIII-D and other plasmas (e.g. [27–30]). Two general conclusions emerge from these calculations. (1) In both the edge and the core, when the friction force is much less than the parallel viscous force, the deuterium and carbon ions rotate in opposite directions with different magnitudes, but when the friction force is much greater than the viscous force then both species rotate in the same direction with similar magnitudes (calculations reporting such results are given in [27–30]). (2) In the plasma edge, the measured carbon rotation velocity is predicted (by the models described in [27] and the references therein) reasonably well in the flattop region, but is significantly over-predicted in the steep gradient region, probably indicating that a retarding torque (ion orbit loss? or viscous influx from SOL flows?) needs to be added to the model.

We note that the measurement of carbon and main ion poloidal rotation in a DIII-D helium plasma [31] (in which both the main and impurity ion velocities can be measured) found the two species to be rotating in opposite directions, indicating plasma conditions such that the viscous force dominated the friction force in this shot. A calculation based on a trace-impurity limit of the Hirshman–Sigmar model [32], in which the carbon viscosity term was neglected in the carbon equation, also predicted the two species to be rotating in different directions. However, these results cannot be generalized to other shots in DIII-D with different relative strengths of the parallel viscous and friction forces, as the calculations of [27–30] indicate.

For the shots examined in this paper, when the deuterium poloidal rotation term in the pinch velocity is evaluated using the measured carbon rotation velocity, its contribution to the pinch velocity subtracts from the contribution of the E_{rad} term. If the calculated deuterium rotation velocity, which is of the opposite sign, is used instead, the deuterium poloidal rotation term reinforces the E_{rad} term, leading to a much larger pinch velocity magnitude (see [30] for details of such a calculation for a DIII-D shot similar in many respects to the one being interpreted in this paper). Thus, we are left with the options of either (i) underestimating the effect on the pinch velocity by using the measured carbon velocity to evaluate the deuterium velocity term in the pinch velocity, or (ii) using the calculated deuterium velocity (perhaps corrected for the difference in the measured and calculated carbon velocities [30]) to evaluate the pinch velocity, which may significantly over-estimate the pinch velocity. We chose the first option

in order to obtain a lower bound on the pinch velocity effect being investigated and to avoid the possibility of widely overestimating the pinch velocity effect. If this conservative estimate yields a significant difference in the pinch velocity between the H-mode and RMP discharges, which it does, then the actual difference in pinch velocity is expected to be larger and more significant.

References

[1] Snyder P.B., Wilson H.R., Osborne T.H. and Leonard A.W. 2004 *Plasma Phys. Control. Fusion* **46** A131
[2] Luxon J.L. 2002 *Nucl. Fusion* **42** 614
[3] Loarte A. *et al* 2003 *Plasma Phys. Control. Fusion* **45** 1549
[4] Liang Y. *et al* 2007 *Phys. Rev. Lett.* **98** 265004
[5] Evans T.E. *et al* 2004 *Phys. Rev. Lett.* **92** 235003
[6] Evans T.E. *et al* 2005 *Nucl. Fusion* **45** 595
[7] Burrell K.H. *et al* 2005 *Plasma Phys. Control. Fusion* **47** B37
[8] Evans T.E. *et al* 2006 *Phys. Plasmas* **13** 056121
[9] Moyer R.A. *et al* 2005 *Phys. Plasmas* **12** 056119
[10] Jackson G.L. *et al* 2003 *Proc. 30th EPS Conf. on Controlled Fusion and Plasma Physics (St Petersburg, Russia)* pp 4–47 (CD-ROM)
[11] Maingi R. *et al* and the NSTX team 2009 *Phys. Rev. Lett.* **103** 075001
[12] Evans T.E. *et al* 2008 *Nucl. Fusion* **48** 024002
[13] Unterberg E.A., Schmitz O., Evans T.E., Maingi R., Brooks N.H., Fenstermacher M.E., Mordijck S., Moyer R.A. and Orlow D.M. 2010 *Nucl. Fusion* **50** 034011
[14] Evans T.E. *et al* 2006 *Nature Phys.* **2** 419
[15] Osborne T.H. *et al* 2008 *J. Phys.: Conf. Ser.* **123** 012014
[16] Stacey W.M. and Evans T.E. 2006 *Phys. Plasmas* **13** 112506
[17] Stacey W.M. and Groebner R.J. 2009 *Phys. Plasmas* **16** 102504
[18] Stacey W.M. 2008 *Contrib. Plasma Phys.* **48** 94
[19] Stacey W.M. and Groebner R.J. 2008 *Phys. Plasmas* **15** 012503
[20] Unterberg E. *et al* and TEXTOR team 2007 *J. Nucl. Mater.* **363–365** 698
[21] Schmitz O. *et al* and TEXTOR team 2009 *J. Nucl. Mater.* **390–391** 330
[22] Tokar M.Z., Evans T.E., Singh R. and Unterberg B. 2008 *Phys. Plasmas* **15** 072515
[23] Rozhansky V., Kaveeva E., Molchanov P., Veselova I., Coster D., Kirk A., Lisgo S. and Narden E. 2010 *Nucl. Fusion* **50** 034005
[24] Kikuchi Y. *et al* 2006 *Phys. Rev. Lett.* **97** 085003
[25] Koslowski H.R. *et al* 2006 *Plasma Phys. Control. Fusion* **48** B53
[26] Militello F. and Waelbreck F.L. 2009 *Nucl. Fusion* **49** 065018
[27] Stacey W.M. 2008 *Phys. Plasmas* **15** 012501
[28] Stacey W.M. 1992 *Phys. Fluids* B **4** 3302
[29] Stacey W.M., Johnson R.W. and Mandrekas J. 2006 *Phys. Plasmas* **13** 062508
[30] Stacey W.M. and Groebner R.J. 2010 Evolution of the H-mode edge pedestal between ELMs *Nucl. Fusion* submitted
[31] Kim J., Burrell K.H., Gohill P., Groebner R.J., Kim Y.-B., St. John H.E., Seraydarian R.P. and Wade M.R. 1994 *Phys. Rev. Lett.* **72** 2199
[32] Kim Y.B., Diamond P.H. and Groebner R.J. 1991 *Phys. Fluids* B **3** 2050